Fortschr. Phys. **48** (2000) 5−7, 623−636

Addressing and Cooling of Single Ions in Paul Traps

H. C. Nägerl*), Ch. Roos, H. Rohde, D. Leibfried, J. Eschner,
F. Schmidt-Kaler and R. Blatt

Institut für Experimentalphysik, Universität Innsbruck,
Technikerstraße 25, A-6020 Innsbruck, Austria

Abstract

The use of cold trapped ions for quantum information processing requires the preparation of linear strings of ions at low temperatures and the coherent manipulation by laser light of the quantum state of individual ions in the string. In our experiment, $^{40}Ca^{+}$ ions are trapped in a linear Paul trap, forming crystallized linear strings when laser cooled. These strings are observed by fluorescence detection on the $S_{1/2}$-$P_{1/2}$ dipole transition at 397 nm using a photomultiplier and a CCD camera. The narrow $S_{1/2}$-$D_{5/2}$ quadrupole transition at 729 nm is used to investigate and manipulate the vibrational motion of the ion in the trap. The spectral resolution obtained up to now on this transition is $2 \cdot 10^{-12}$, proving long coherence time of the two-level system. Addressing of individual ions in the string is achieved, using a tightly focused laser beam at 729 nm, and detected by the observation of quantum jumps from the $S_{1/2}$ to the $D_{5/2}$ level. These experimental techniques make ions in a superposition of their $S_{1/2}$ and $D_{5/2}$ states suitable as qubits for quantum information processing. The realization of a two-ion quantum gate furthermore requires ground-state cooling of the string. The status of current experiments is reviewed and techniques to achieve ground-state cooling of ion strings are discussed.

1. Introduction

One or a few ions stored in a radio-frequency Paul trap offer an ideal environment to study the dynamics of simple quantum systems. With the aid of laser pulses, the investigator can taylor the interaction of this system almost at will. Quantum information processing, as well as the study of foundations of quantum mechanics, ultrahigh precision spectroscopy, and the investigation of future frequency standards, and last but not least the investigation of decoherence, are possible applications of the perfect control of internal and external quantum mechanical degrees of freedom of a string of trapped ions [1−5]. A particulary interesting situation arises when a suitable laser light field couples the motion of the ion(s) in the trapping potential with their electronic levels. This situation is described by an interaction Hamiltonian acting on two internal electronic levels, $|s\rangle$ and $|d\rangle$, with energy difference ω_{sd}, which are 'dressed' by the harmonic oscillator states $|n\rangle$ of the external motion at frequency ω_{trap} (see Fig. 1). The interaction Hamiltonian takes the form

$$H_{\text{int}} = -\hbar\Omega(\sigma^{+}\, e^{i\eta(a^{\dagger}+a)} + \sigma^{-}\, e^{-i\eta(a^{\dagger}+a)}), \tag{1}$$

where $\eta = k\sqrt{\hbar/2m\omega_{\text{trap}}}$ is the Lamb Dicke parameter, $(a^{\dagger}+a)$ the position operator in terms of creation and annihilation operators for the harmonic oscillator, and Ω is the coupling strength proportional to the amplitude of the laser light field. This interaction Hamiltonian is inherently richer than the classical Jaynes Cummings Hamiltonian [6−9], but

*) Present address: California Institute of Technology, Dept. of Physics (12-33), 1200 E. California Blvd., Pasadena, CA 91125

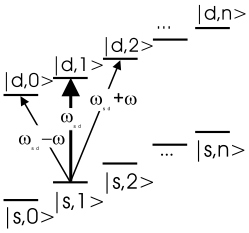

Fig. 1: Electronic states of a two-level atom $|s\rangle$ and $|d\rangle$, 'dressed' by the number states of its quantized motion.

reduces to the latter in the so-called Lamb-Dicke limit

$$\eta \cdot \sqrt{\langle (a^\dagger + a)^2 \rangle} = \eta \cdot \sqrt{2n+1} \ll 1 \tag{2}$$

and when the detuning of the light field with respect to ω_{sd} is $\delta = -\omega_{\text{trap}}$. We assume that the radiative width of both levels $|s\rangle$ and $|d\rangle$ is much smaller than ω_{trap}, such that the motional sidebands of the atomic resonance, $|s,n\rangle$ to $|d,n\pm 1\rangle$, are well resolved. In general, any detuning $\delta = (n'-n)\cdot\omega_{\text{trap}}$ (n, n' integer numbers) will resonantly drive transitions between the states $|s,n\rangle$ and $|d,n'\rangle$, and thus lead to a different interaction Hamiltonian.

2. Ion trapping

The experimental techniques to realize a well controlled situation described by the Hamiltonian above [10−16] have historically evolved from efforts to build frequency standards with trapped and cooled ions [17−19]. Dynamical trapping of charged particles in radio-frequency (rf) traps has been first proposed and experimentally verified by W. Paul in 1958 [20]. An rf electric field, generated by an appropriate electrode structure, creates a pseudo-potential confining a charged particle [21]. For the trapping of single ions the electrodes typically have dimensions of a few millimeters down to about 100 μm. The rf fields are in the 1−300 MHz range, with amplitudes of hundreds of Volts. The motion of a particle confined in such a field consists of a fast component synchronous with the applied driving field (micromotion), which disappears at the node of the rf field, and a slow (secular) motion in the dynamically created pseudo-potential. For a quadrupole rf field geometry, the pseudo-potential is harmonic and the quantized secular motion of the trapped ion is very accurately described by a quantum harmonic oscillator.

In a *linear* Paul trap, the quadrupole rf field exists only in the xy-plane, such as in a quadrupole mass spectrometer, and an additional electrical dc potential provides confinement along the z-axis (see Fig. 2). A major advantage compared to a three-dimensional Paul trap is that the micromotion completely vanishes for all ions on the z-axis. Furthermore the oscillation frequency in that direction can be chosen freely and independently from the radial secular frequencies. In contrast, in three-dimensional Paul traps Coulomb repulsion between ions pushes them into the rf field where micromotion heating occurs. Linear Paul traps presumably avoid compeltely this heating source even for long linear strings of ions. However, even if the use of linear traps for a larger number of ions seems favorable, an elongated version of the three-dimensional Paul trap has been used to produce strings of two and three ions [22].

Our trap [23] consists of 4 parallel steel rods with 2 mm spacing, diagonally connected to generate the quadrupole rf field for radial confinement. The rf field at $\Omega/2\pi = 18$ MHz yields a radial trapping pseudo-potential with secular frequencies of $\omega_r = 1.4$ MHz. Two DC ring electrodes of 4mm diameter and 10mm spacing serve as the axial endcaps for longitudinal confinement. DC voltages on the ring electrodes result in a harmonic trapping potential at an

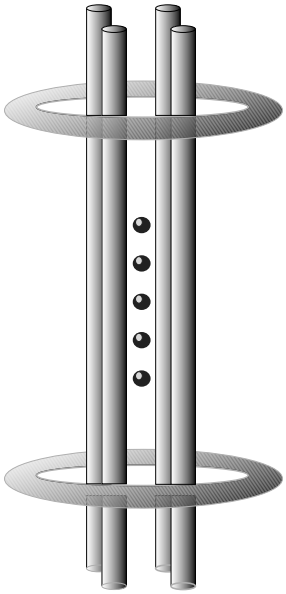

Fig. 2: Schematic setup of the linear Paul trap.

axial frequency of $\omega_z = 100-500$ kHz. The relatively large dimensions of our trap help to reduce unwanted interactions between the ion string and surface charges on the electrodes and thus reduce heating [24]. Ions are produced from an atomic beam by electron impact ionization inside the trap, where they are subsequently confined and laser cooled [25, 26].

3. Laser cooling

We have chosen $^{40}Ca^+$ ions for the experiments since their excitation wavelengths are relatively easy to generate with solid state and diode lasers. See Fig. 3 for the relevant energy levels.

Laser light at 397 nm is generated with a frequency doubled Ti : Sapphire laser at 793 nm while the light sources at 866 nm, 854 nm and 850 nm are grating stabilized diode lasers. For Doppler cooling of the Ca^+ ions we use the dipole-allowed $S_{1/2}$-$P_{1/2}$ transition at 397 nm, and we reach a temperature near the Doppler cooling limit of 0.5 mK. Fluores-

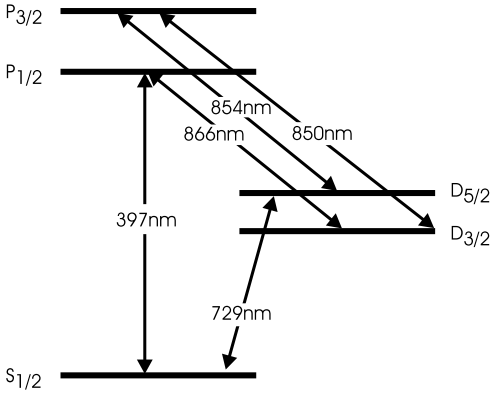

Fig. 3: Level scheme of $^{40}Ca^+$. The lifetime of both D states is 1 s. Superposition states of $|S_{1/2}\rangle$ and $|D_{5/2}\rangle$ are used to implement a qubit.

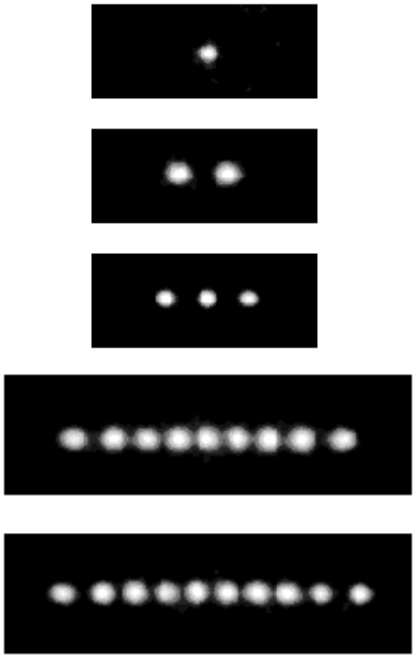

Fig. 4: Examples of linear strings of ions at $\omega_z = 125$ kHz, leading to adistance between two ions of 19 μm. The exposure time of the CCD camera was 1s.

cence light of the ions at 397 nm is collected through two optical viewports using f/1.3 collimation lenses at a working distance of 65mm. One lens images the spatially integrated fluorescence onto a photomultiplier, and the second lens images the ion string onto an intensified CCD camera with 20-fold magnification. Here we observe linear ion strings of up to 15 ions, with distances between the ions of 19 μm (2 ions) to 7 μm (15 ions). See Fig. 4 for an image of 1, 2, 3, 9, and 10 ions. The optical resolution for the detection of fluorescence light at 397 nm has been measured to be 4 μm [23].

Further cooling beyond the Doppler limit of 0.5 mK is possible in the $^{40}Ca^{+}$ ion by sideband cooling [27–29] on the quadrupole $S_{1/2}$-$D_{5/2}$ transition at 729 nm. The light exciting this transition is generated by a frequency stabilized Ti : Sapphire laser. Additionally, we shine light at 854 nm onto the ions to quench the metastable $D_{5/2}$ state and thus increase the cooling rate. Please note that sideband cooling is much simpler if the initial state after Doppler cooling is well within the Lamb Dicke regime (see Fig. 5). This condition is fulfilled if the trap frequency in z-direction is above 500 kHz such that $\eta \leq 0.5$ and the average vibrational quantum number at the Doppler limit is $\langle n \rangle_{\text{therm.}} \leq 20$.

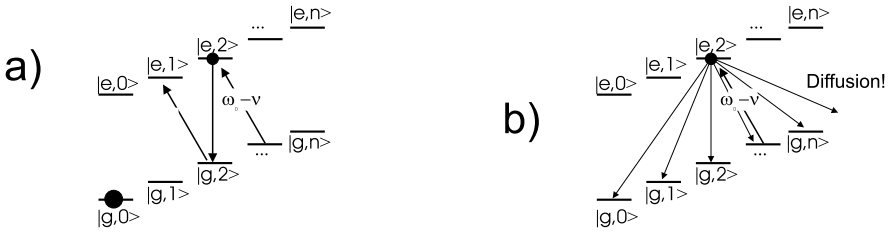

Fig. 5: a) Scheme of sideband cooling inside the Lamb Dicke regime. The cooling laser is red detuned from the bare atomic resonance by ω_z. b) red sideband excitation outside the Lamb Dicke limit leads to strong diffusion and heating.

4. Normal modes of oscillation

In a linear ion trap, ions can be confined and optically cooled such that they form ordered structures [30, 31]. If the radial confinement is strong enough such that $\omega_r/\omega_z > 0.73\mathrm{N}^{0.86}$, N ions arrange in a linear string along the trap axis at distances determined by the equilibrium of their Coulomb repulsion and the axial dc potential . If this potential is sufficiently harmonic, the positions can be described by a single parameter, the axial frequency ω_z. Small displacements of the ions from their equilibrium positions are described in terms of normal modes. As an example, consider two $^{40}Ca^{+}$ ions confined in a linear ion trap: The first normal mode corresponds to an oscillation of both ions moving back and forth as if they were rigidly joined. This oscillation is referred to as the *center-of-mass* (COM) *mode* of the string. The second normal mode corresponds to an oscillation where the two ions move in opposite directions. More generally, this so-called *breathing-mode* describes a string of N ions moving with an amplitude proportional to their mean distance from the trap center. Explicit calculation of the normal modes and the respective eigenfrequencies of an ion string yields the following results [32, 33]: i) for a one-dimensional string consisting of N ions there are N normal modes and normal frequencies, ii) the frequency of the center of mass mode is equal to the frequency of a single ion, iii) higher order frequencies are nearly independent of the ion number N and are given by $(1, \sqrt{3}, \sqrt{29/5}\,, 3.05(2), \ldots) \cdot \omega_z$, where the numbers in brackets indicate the maximum frequency deviation as N is increased from 1 to 10 ions, iv) the relative amplitudes of the normal modes have to be evaluated numerically, at least for strings with more than 3 ions, see equation (28) in Ref. [32].

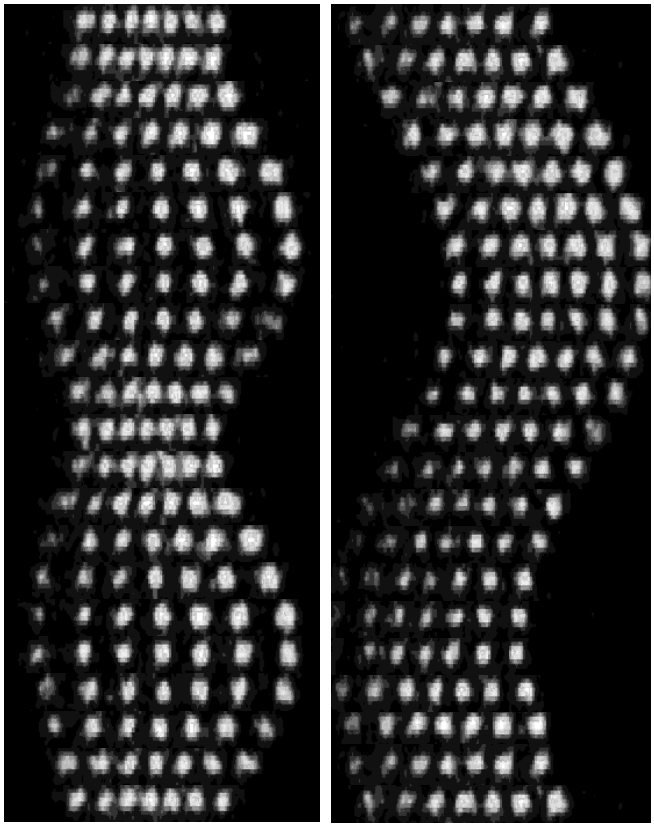

Fig. 6: Stroboscopic image of the rf-excited center-of-mass motion at 158.5 kHz (right) and breathing mode motion at 276.0 kHz (left).

After loading the trap with a string of ions, we excited normal modes by applying additional ac-voltages to one of the ring electrodes [34]. The normal mode oscillation has been observed stroboscopically with the gated CCD camera that accumulates images at the same phase of the exciting electric field. The measured excitation frequency for the breathing mode agrees within 1% with the expected frequency of $\sqrt{3}$ times the center-of-mass frequency. Fig. 6 shows the excitation of the center of mass mode (158.5 kHz) for a string of seven ions and the excitation of the breathing mode (276.0 kHz). In order to excite the breathing mode it was necessary to apply voltages about 300 times higher than the ones needed for excitation of the center of mass mode. Excitations of higher order modes other than the breathing mode were not observed with the available ac-voltages. This is due to the fact that the exciting field is nearly uniform along the ion string so that higher modes, which need field gradients across the ions are excited much less efficiently. The COM vibration is excited with a uniform field and is therefore very susceptible to field fluctutations. In contrast, the excitation of higher order modes by field fluctuations is less likely since the spatial field variation is very small on the length scale given by the ion distance. Therefore, this unwanted heating process occurs less strongly for the higher order modes.

5. Electron shelving

The basic idea of the 'electron shelving' method as proposed by Dehmelt [35] is very simple: It requires a three-level system consisting of a ground state $|s\rangle$, a metastable excited state $|d\rangle$, and a short lived excited state $|p\rangle$. A laser pulse couples the ground state to the excited state $|d\rangle$, leaving the system in a superposition $\alpha|s\rangle + \beta|d\rangle$. If now the $|s\rangle \rightarrow |p\rangle$ transition is driven, the short lived state $|p\rangle$ will be excited and scatter photons if, and only if, the system collapses into $|s\rangle$. The state reduction happens already with the first scattered photon even if it is not observed. The measurement yields the result $|s\rangle$ with probability $|\alpha|^2$, corresponding to the observation of photons, or the result $|d\rangle$ with probability $|\beta|^2$, corresponding to the absence of photons. Even if the efficiency for detecting the photon from one decay of $|p\rangle$ is low (typically 10^{-3}) one can keep re-exciting the system and scatter millions of photons, eventually detecting a few of them in case the state is reduced to $|s\rangle$. If the state is 'shelved' in the metastable state $|d\rangle$, no fluorescence will happen. In every single experiment the answer will be either $|s\rangle$ – photons detected – or $|d\rangle$ – no photons detected –, thus distinguishing these states with 100% detection efficiency and

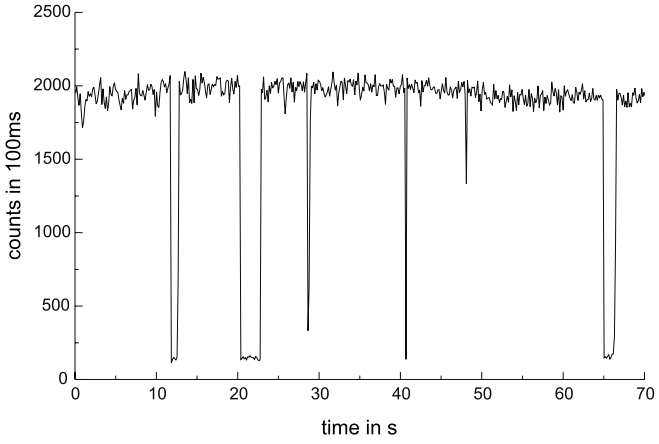

Fig. 7: Quantum jumps of a single $^{40}Ca^{+}$ ion. When the ion makes a transition to the metastable $D_{5/2}$ state, the fluorescence drops. After an average time equal to the lifetime of the excited state ($\tau \simeq 1$ s), a spontaneous transition returns the ion to the ground state and the fluorescence reappears.

destroying all coherences between them. Averaged over many experiments, the number of tries where fluorescence photons are observed will be proportional to $|\alpha|^2$. As an example of the efficiency of this method, Fig. 7 shows the fluorescence signal from a single Ca^+ ion during continuous excitation on the $S_{1/2} \rightarrow P_{1/2}$ transition at 397 nm and the $S_{1/2} \rightarrow D_{5/2}$ transition at 729 nm. While the ion is in the $S_{1/2}$ or $P_{1/2}$ state it radiates about 2000 photons in 100 ms into the photomultiplier. At certain times, the ion is excited into the $D_{5/2}$ state by the beam at 729 nm and the rate drops to about 150 events in 100 ms, given by the number of dark counts of the imperfect photomultiplier, and some 397 nm light directly scattered from the exciting beam into the detector. Obviously, the two states can be discriminated with excellent precision already within one ms. The average dark time is about 1 second, the radiative lifetime of the $D_{5/2}$ state. In the language of quantum information processing, this two-level system of $S_{1/2}$ state and $D_{5/2}$ state represents an ideal qubit, several of them form a quantum register.

For such a possible realization of a quantum register, the observation of fluorescence with the intensified CCD camera yields the internal state detection with 100% probability: The sites of the ions in the string appear bright or dark depending on the logic state of each qubit.

6. Spectroscopy of the $S_{1/2}$–$D_{5/2}$ transition

For quantum information processing, the dressed quantum states of the qubits are coherently manipulated using laser pulses similar to the $\pi/2$-pulses used in optical Ramsey spectroscopy. To investigate this technique with a single ion, we first used laser pulses of fixed length at 729 nm that couple the $S_{1/2}$ and $D_{5/2}$ states. A magnetic field is used to split the transitions to different m_J levels in frequency. After preparing the $S_{1/2}, m_J = +1/2$ substate by optical pumping, we excite the ion to the $D_{5/2}$ state manifold of Zeeman sublevels. We are mainly interested in the $S_{1/2} \rightarrow D_{5/2}$, $m_J = +1/2 \rightarrow +5/2$ transition which has the largest Clebsch-Gordon coefficient. In the third step of this 'quantized spectroscopy', see Fig. 8, we detect whether a transition to the shelving level $D_{5/2}$ has been induced. The above sequence is repeated typically 100 times to measure the excitation probability P_D for any set of parameters, In this way we study the dependance of P_D on the experimental parameters such as the detuning of the light at 729 nm with respect to the ionic transition or the length of the excitation puls. The duration of a single sequence is typically 5 ms or less, and we can syncronize the sequence with the ac power line at 50 Hz, which reduces ac-magnetic field fluctuations, although at the cost of slower data aquisition.

As a consequence of the harmonic ladder of 'dressed' ion states (Fig. 1), the spectrum of excitation $P_D(\nu)$ vs δ_{729}, Fig. 9, shows a central peak with equidistant sidebands at multi-

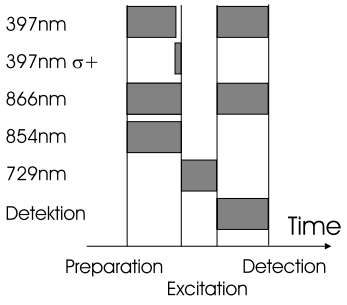

Fig. 8: Experimental sequence for the quantized spectroscopy, see text for details.

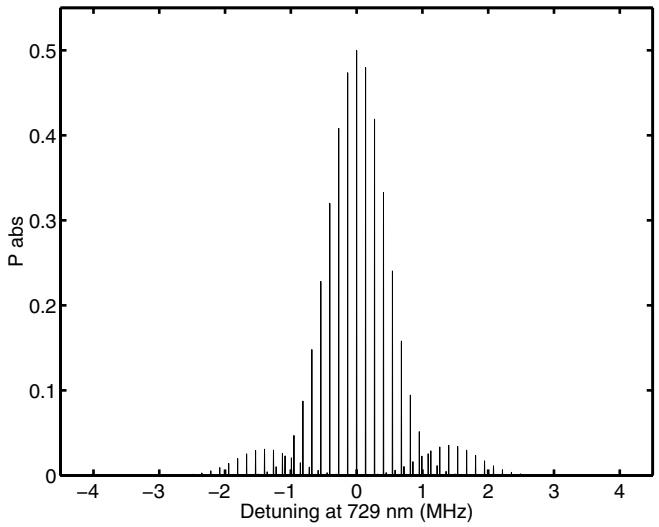

Fig. 9: Calculated sideband spectrum for excitation of the $S_{1/2}$ to $D_{5/2}$ transition, for one ion below saturation and at the Doppler cooling limit. Oscillation frequencies are $\omega_z = 136$ kHz, $\omega_r = 1.4$ MHz. The radial sidebands are magnified by a factor of 10.

ples of the trap frequencies. The width of the envelope corresponds to the ion temperature that was assumed for this simulation to be at the Doppler limit of 0.5 mK and $\eta = 0.25$.

The measured sideband spectra in Fig. 10 show equidistant sidebands at the trap frequency on the z-axis. Increasing the voltages on the ring -shaped endcap electrodes increases the trap frequency. The only resonance that does not shift corresponds to excitation on the carrier (without change in phonon number: $n \rightarrow n$). The observed linewidth for the transition on the carrier has been measured to be 1 kHz ($\delta\nu/\nu = 2 \cdot 10^{-12}$) in the ac-power-line synchronized aquisition mode. The inverse of this measured linewidth, 1ms, gives the upper limit for any coherent operation, and we are currently working to further improve this limit. The main limitations are the fluctuations of the magnetic field at the ions position and the phase fluctuations of the Ti : Sapphire laser at 729 nm.

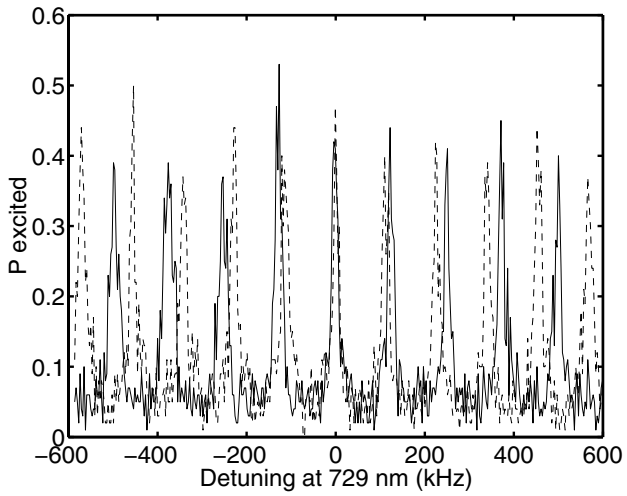

Fig. 10: Shift with trap frequency of the low-order sidebands adjacent to the carrier, as observed with one ion. The dashed line shows the spectrum as measured with a trap stiffness corresponding to $\omega_z = 113.8$ kHz. For the solid line, the ring voltages were increased by about 10 V, resulting in an increase of ω_z to 124.1 kHz. No ac-power line synchronization was used.

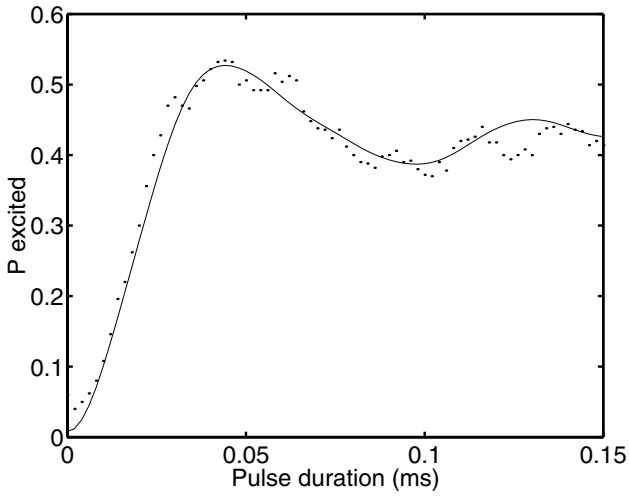

Fig. 11: Rabi oscillations between $|S_{1/2}, n\rangle$ and $|D_{5/2}, n\rangle$ for a single ion in the linear trap. The solid curve is a plot of equation (3) with Lamb-Dicke parameter $\eta = 0.25$, Rabi frequency $\Omega = 2\pi \cdot 50$ kHz, and thermal occupation number $\langle n_{\text{therm.}} \rangle = 500$.

7. Driving coherent dynamics

A major requirement for quantum information processing is the ability to apply laser pulses of certain duration to implement qubit rotations of $\pi/2$, π and 2π [4]. We have experimentally varied the puls length of excitation on the carrier and measured the $D_{5/2}$ state probabilty $P_D(t)$ (see Fig. 11). The theoretical curve which fits the data takes the different Rabi

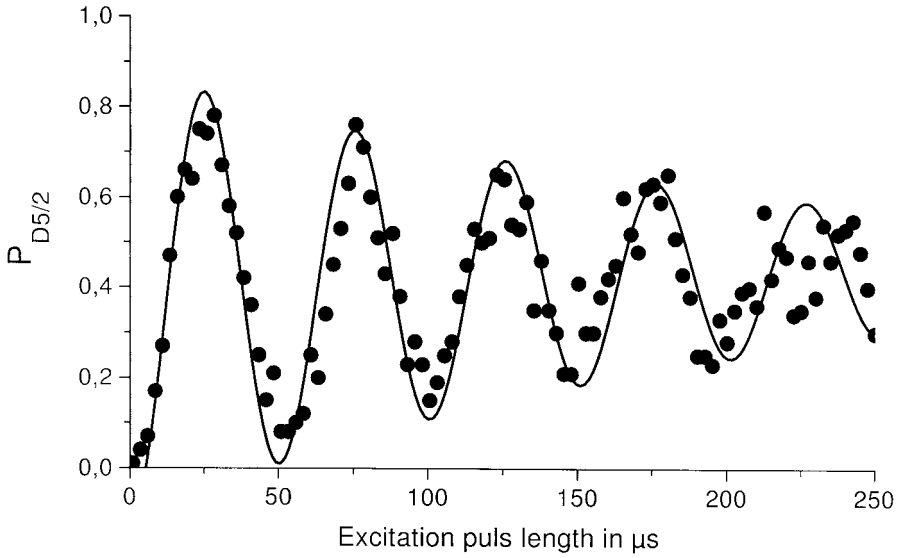

Fig. 12: Rabi oscillations as in Fig. 11, measured in a three-dimensional Paul trap with higher trap frequency $\omega = 0.9$ MHz with a single Doppler cooled ion. The solid curve is calculated with $\eta = 0.09$, $\Omega = 2\pi \cdot 11.4$ kHz, and $\langle n_{\text{therm.}} \rangle = 11.6$. The Doppler cooling limit for this trap is $\langle n \rangle \approx 10$.

frequencies Ω_{nn} for the transitions $|s,n\rangle$ to $|d,n\rangle$ into account.

$$P_D(t) = \sum_{n=0}^{\infty} p_n \cdot \sin^2(\Omega_{nn} \cdot t), \tag{3}$$

$$\Omega_{nn} = \Omega \cdot e^{-\eta^2/2} \cdot \mathcal{L}_n^0(\eta) \tag{4}$$

where p_n denotes the phonon probability distribution and $\mathcal{L}_n^0$ a Laguerre polynomial. The oscillating dependence of Ω_{nn} on n and the large mean thermal vibration number $\langle n \rangle$, as typical for the relatively weak z-confinement of the linear Paul trap, are responsible for the fast dephasing we observe. Here, after Doppler cooling, the ion is *not* found in the Lamb-Dicke regime. We emphasize that the dephasing is *not* due to laser frequency fluctuations which limit coherent dynamics only on a timescale of 1ms. This is also proven by a similar measurement of Rabi oscillations that we performed in a three-dimensional single ion Paul trap with much tighter binding (see Fig. 12). Four Rabi oscillation periods are clearly visible and the dephasing is again mainly due to the summation of different frequencies Ω_{nn}.

In a series of exciting experiments, the ion storage group around D. Wineland has used coherent dynamics for the generation and investigation of nonclassical phonon states [36], the implementation of a controlled-NOT gate [37], measurements of the Wigner function [38], and experiments on Schrödinger cat states temporal decoherence [39].

8. Individual addressing of ions in a string

Taking advantage of the high optical resolution of the lens for the collection of fluorescence in our experiment, we use the same optical path also for individual addressing (see Fig. 13). The ingoing laser beam at 729 nm is separated from the outgoing uv fluorescence with a dichroic mirror. An optical fiber between laser and trap setup provides stable alignment, and a telescope is used to adjust the $\lambda = 729$ nm beam parameters for optimum focusing. Between fiber exit and telescope, an acousto-optical modulator (AOM 1) is used to shift the direction of the addressing beam and thus to allow focusing onto the

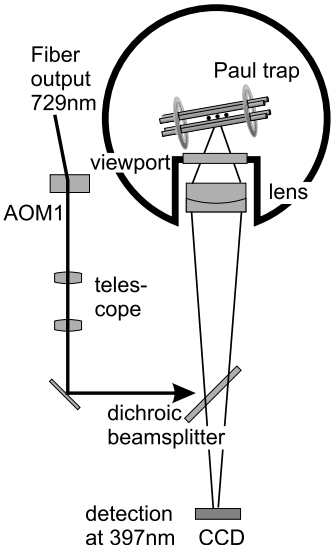

Fig. 13: Scheme of the experimental setup to address single ions in a string. Laser light at 729 nm from an optical fiber is superimposed with the (counterpropagating) fluorescence at 397 nm on a dichroic beamsplitter. Thus, the laser is focused by the objective lens onto the ion string. A two-lens telescope transforms the fiber output for optimum focussing. To address different ions in the string, either the acousto-optical modulator (AOM1) is used to shift the direction of the laser beam, or the ions are shifted with additional dc potentials on the ring electrodes.

different ions. The ion string is illuminated by the addressing laser under an angle $\alpha = 67.5$ degree to the trap axis in order to allow qubit excitation together with excitation of vibrational modes at frequency ω_z. In this geometry, we calculate a Lamb Dicke parameter $\eta = \sqrt{\hbar k^2 \cos^2(\alpha)/2m\omega_z} = 0.17$ for the center-of-mass motion.

We have experimentally demonstrated two ways of addressing single ions in the string with a string of 3 ions [40]: First, we used the tightly focused 729 nm laser beam at a fixed position and shifted the ion string by slight variation (less than 1%) of the endcap ring electrode voltages while the variation of the ion string position was monitored on the CCD camera. Secondly, we fixed the ion string position and moved the laser beam over the string with the AOM1. The optical excitation sequence consists of three parts: A 0.5 ms excitation period with light at 729 nm is followed by a detection period with the laser at 397 nm and 866 nm on (2ms), during which we register the quantum jump probability P_D to the metastable $D_{5/2}$ level. The sequence is closed by a cooling and repumping period with the lasers at 397 nm, 866 nm and 854 nm on (2 ms). During the excitation period, we use a weak beam at 397 nm to spectrally broaden the narrow $S_{1/2}$-$D_{5/2}$ transition. This excitation sequence is repeated 100 times, thus yielding a value for the P_D. The average of 15 such measurements is plotted versus the center position of the ion string in Fig. 15. From a fitted Gaussian function $A_0 + \sum A_i \exp[-2((x - x_i^0)/w_i)^2]$ with height A_i, position x_i^0, and width w_i corresponding to the three peaks in the signal and background A_0, we obtain a spatial resolution of addressing of $w = 5.6(0.2)$ μm. This width of the Gaussian is mostly due to the optical properties of the addressing channel, since the Ca^+ ion wave packet has a calculated width of $\sqrt{\delta x^2} = 1.6$ μm at 5 mK. For exact calibration of the CCD pixel size we used a resonant excitation of the center-of-mass mode of the ion string [34] (see section IV). From the measured frequency of 125(0.2) kHz we obtain an equilibrium distance between the ions of 19.12(0.02) μm [32]. Thus, we can exactly calibrate the pixel size of the recorded CCD images to 1.12 μm per pixel. In Fig. 15(b)–(d) we show CCD images of the addressed string, with different ions transferred to the non-fluorescing $D_{5/2}$ state. Assuming a Gaussian intensity distribution, the intensity of the addressing beam at the position of a neighbouring ion 9 μm away would be as small as 1%.

After having shown sufficiently good spatial resolution for individual addressing, we implemented a scheme that would be directly applicable to future quantum information processing. Shifting the ion string does not allow sufficiently fast switching for longer ion strings, since a fast, non-adiabatic shift of position would presumably cause heating [24]. For fast addressing, the laser beam position is shifted by an acousto-optical modulator

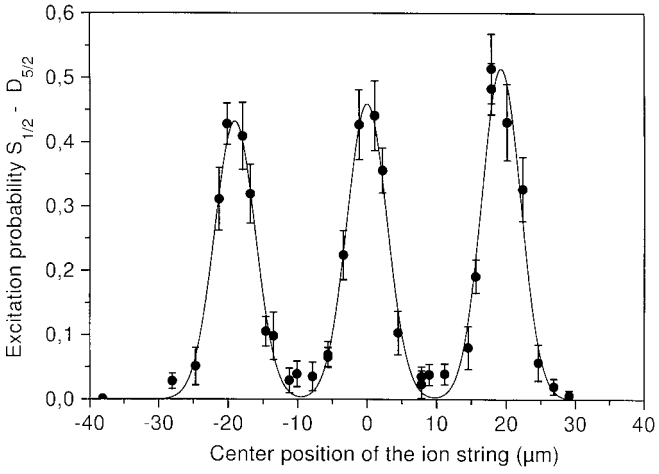

Fig. 14: Quantum jump rate from the $S_{1/2}$ to the $D_{5/2}$ state induced by a tightly focused laser beam at 729 nm. The ion string position is varied while the laser waist remains fixed. Individual ions are resolved by the addressing beam with a Gaussian width of $w = 5.6(0.2)$ μm. See Fig. 15 for CCD images of the string that were taken simultaneously. The error bars indicate the one sigma deviations from 15 measurements.

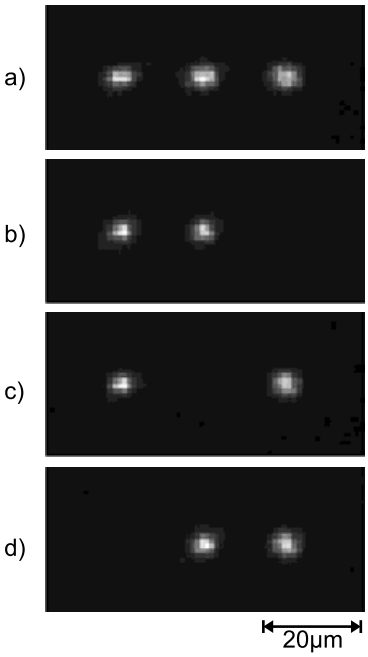

Fig. 15: (a): Fluorescence at 397 nm of three ions imaged onto the CCD camera. The distance between ions is 19.12(0.02) μm ($\omega_z = 125(0.2)$ kHz) and the spatial resolution is near 4 μm. The exposure time is 1s. (b)−(d): Different ions in the string are addressed with focused laser light at 729 nm and transferred into the non-fluorescing $D_{5/2}$ state.

(AOM 1) and thus focused on different ions. The associated change in frequency is compensated by a second double-pass acousto-optical modulator in front of the fiber. We measured an addressing resolution as good as in the first addressing scheme using static fields.

9. Conclusion

Currently we modify our linear Paul trap to find optimum conditions for individual addressing *and* sideband cooling. The obtained addressing resolution permits us to work with higher longitudinal trap frequencies of 500 kHz−1 MHz at inter-ion distances of 8−6 μm. With such trapping parameters we will be in the Lamb Dicke regime already after Doppler cooling. Switching between the ions within μs is feasible and will allow roughly 10 operations within the coherence time of 1ms that we measured from heigh resolution spectroscopy on the $S_{1/2}$-$D_{5/2}$ transition [41]. Apart from the 'classical' proposal by I. Cirac and P. Zoller for quantum logic gates [4], A. Sörensen and K. Mölmer recently proposed a scheme which uses ions in thermal motion inside the Lamb Dicke regime [42, 43] which could be implemented in our setup. The novel addressing technique will further allow us to investigate selectively the temperature and heating rate [24] for different vibrational modes, and for ions at different locations in the ion string. It will furthermore be used for precision frequency measurements on ions at different locations in a linear string. The specification of optical clock transitions will use the measurement of micromotion [44] for ions at different positions in the string to determine and eventually correct the corresponding frequency shifts. This should be as well interesting for the investigation of time standards based on trapped ions.

Stored ions in three-dimensional or linear Paul traps provide a versatile tool for quantum information processing. We have given a description of experimental techniques for the storage, observation, cooling, individual addressing, and coherent manipulation of ions in linear strings. For future experiments, the advantages of ion trapping techniques such as −

scalabilty from 1 to N ions in a string, the use of different vibration modes, long coherence times, and the 100% state detection probability – seem to be very promising for quantum information processing.

This work is supported by the Fonds zur Förderung der wissenschaftlichen Forschung (FWF) as project No. P11467 and within the Spezialforschungsbereich SFB 15, and in parts by the TMR networks "Quantum Information" (ERB-FMRX-CT96-0087), and "Quantum Structures" (ERB-FMRX-CT96-0077).

References

[1] A. Ekert, in Atomic Physics **14**, 450, ed. D. J. Wineland, C. Wieman, S. J. Smith, AIP New York 1995; S. Haroche et. al., in Atomic Physics **15**, 1; J. I. Cirac, S. Gardiner, T. Pellizari, J. Poyatos, P. Zoller et. al., in Atomic Physics **15**, 16; D. J. Wineland et. al., in Atomic Physics **15**, 31, ed. H. B. van den Heuvell, J. T. M. Walraven, M. W. Reynolds , AIP New York 1996.
[2] The Physics of Quantum Information, ed. D. Bouwmeester, A. Ekert, A. Zeilinger, Springer, submitted.
[3] A. Ekert and R. Josza, Rev. Mod. Phys. **68**, 3733 (1997).
[4] J. I. Cirac, P. Zoller, Phys. Rev. Lett. **74**, 4091 (1995).
[5] J. R. Anglin, J. P. Paz and W. H. Zurek, Phys. Rev. A **55**, 4041 (1997).
[6] C. A. Blockey, D. F. Walls, H. Risken, Europhys. Lett. **17**, 509 (1992).
[7] J. I. Cirac, R. Blatt, A. S. Parkins and P. Zoller, Phys. Rev. Lett. **70**, 762 (1993).
[8] J. I. Cirac, R. Blatt, A. S. Parkins and P. Zoller, Phys. Rev. A **49**, 1202 (1994).
[9] J. I. Cirac, R. Blatt and P. Zoller, Phys. Rev. A **49**, R3174 (1994).
[10] http://www.bldrdoc.gov/timefreq/ion/index.htm
[11] http://horology.jpl.nasa.gov/research.html
[12] http://mste.laser.physik.uni-muenchen.de/lg/worktop.html
[13] http://p23.lanl.gov/Quantum/quantum.html
[14] http://dipmza.physik.uni-mainz.de/ www_werth/calcium/calcium.html
[15] http://www-phys.rrz.uni-hamburg.de/home/vms/group_a/index.html
[16] http://heart-c704.uibk.ac.at/
[17] Proc. 5th Symp. Freq. Standards and Metrology, ed. J. C. Bergquist, (World Scientific, 1996).
[18] D. J. Berkeland, J. D. Miller, J. C. Bergquist, W. M. Itano and D. J. Wineland, Phys. Rev. Lett. **80**, 2089 (1998).
[19] R. Blatt, in Atomic Physics **14**, 219, ed. D. J. Wineland, C. Wieman, S. J. Smith, AIP New York 1995.
[20] W. Paul, O. Osberghaus and E. Fischer, Forschungsberichte des Wirtschafts- und Verkehrsministerium Nordrhein-Westfalen **415** (1958).
[21] P. K. Ghosh, Ion traps, Clarendon, Oxford 1995.
[22] B. E. King, C. J. Myatt, Q. A. Turchette, D. Leibfried, W. M. Itano, C. Monroe and D. J. Wineland, Phys. Rev. Lett. **81**, 1525 (1998).
[23] H. C. Nägerl, W. Bechter, J. Eschner, F. Schmidt-Kaler and R. Blatt, Appl. Phys. B **66**, 603 (1998).
[24] D. J. Wineland, C. Monroe, W. M. Itano, D. Leibfried, B. King and D. M. Meekhof, Journal of Research of the National Institute of Standards and Technology **103**, 259 (1998).
[25] D. J. Wineland, W. M. Itano, J. C. Bergquist and R. G. Hulet, Phys. Rev. A **36**, 2220 (1987).
[26] D. J. Wineland and H. Dehmelt, Bull. Am. Phys. Soc. **20**, 637 (1975).
[27] F. Diedrich, J. C. Bergquist, W. M. Itano, D. J. Wineland, Phys. Rev. Lett. **62**, 403 (1989).
[28] C. Monroe, D. M. Meekhof, B. E. King, S. R. Jeffers, W. M. Itano, D. J. Wineland, P. Gould, Phys. Rev. Lett. **74**, 4011 (1995).
[29] B. E. King, C. J. Myatt, Q. A. Turchette, D. Leibfried, W. M. Itano, C. Monroe and D. J. Wineland, Phys. Rev. Lett. **81**, 1525 (1998).
[30] I. Waki, S. Kassner, G. Birkl, H. Walther, Phys. Rev. Lett. **68**, 2007 (1992).
[31] M. G. Raizen, J. M. Gilligan, J. C. Bergquist, W. M. Itano, D. J. Wineland, Phys. Rev. A **45**, 6493 (1992).
[32] D. F. V. James, Appl. Phys. B **66**, 181 (1998).

[33] A. STEANE, Appl. Phys. B **64**, 623 (1997),
[34] H. C. NÄGERL, D. LEIBFRIED, F. SCHMIDT-KALER, J. ESCHNER and R. BLATT, Optics Express **3**, 89 (1998).
[35] H. DEHMELT, Bull. Am. Phys. Soc. **20**, 60 (1975).
[36] D. M. MEEKHOF, C. MONROE, B. E. KING, W. M. ITANO and D. J. WINELAND, Phys. Rev. Lett **76**, 1796 (1996).
[37] C. MONROE, D. M. MEEKHOF, B. E. KING, W. M. ITANO, D. J. WINELAND, Phys. Rev. Lett. **75**, 4714 (1995).
[38] D. LEIBFRIED, D. M. MEEKHOF, B. E. KING, C. MONROE, W. M. ITANO and D. J. WINELAND, Phys. Rev. Lett **77**, 4281 (1996).
[39] C. MONROE, D. M. MEEKHOF, B. E. KING and D. J. WINELAND, Science **272**, 1131 (1996)
[40] H. C. NÄGERL, D. LEIBFRIED, G. THALHAMMER, J. ESCHNER, F. SCHMIDT-KALER and R. BLATT, Phys. Rev. A (1999), accepted for publication.
[41] H. C. NÄGERL et. al., to be published.
[42] A. SOERENSEN and K. MOELMER, Phys. Rev. Lett. **82**, 1971 (1998).
[43] K. MOELMER and A. SOERENSEN, Phys. Rev. Lett. **82**, 1835 (1998).
[44] D. J. BERKELAND, J. D. MILLER, J. C. BERGQUIST, W. M. ITANO and D. J. WINELAND, J. Appl. Phys. **83**, 5025 (1998).